Journal of Solid State Chemistry 182 (2009) 2167–2175

Contents lists available at ScienceDirect

Journal of Solid State Chemistry

journal homepage: www.elsevier.com/locate/jssc

Synthesis, network structure and morphology of s-triazine-organosilane glassy hybrid materials

Isam Arafa *, Mazin Shatnawi, Heyam Sàad

Department of Applied Chemistry, Faculty of Science, Jordan University of Science and Technology, P.O. Box 3030, Irbid 22110, Jordan

ARTICLE INFO

Article history:
Received 14 January 2009
Received in revised form
12 May 2009
Accepted 19 May 2009
Available online 2 June 2009

Keywords:
Hybrid glass
Organosilane
s-Triazine
Hybrid material
Vicat hardness

ABSTRACT

A series of five hybrid materials are synthesized by the reaction of cyanuric chloride ($C_3N_3Cl_3$) with different alkoxysilanes ($R_xSi(OC_2H_5)_{4-x}$, $R = CH_3$, C_6H_5 and $x = 0$, 1, 2) in ethanol using sol–gel technique. The resulting s-triazine-organosilane products were examined using spectroscopic (UV–visible, FT-IR), thermal (thermogravimetric analysis, TGA), powder X-ray diffraction (P-XRD), BET analysis and microscopic (scanning electron microscopy, SEM) techniques. These hybrid materials exhibit globular and two-dimensional morphological textures with varying degrees of crystalline microstructures. Depending on the functionality of the organosilane building blocks the obtained hybrid materials exhibit different material characteristics including their solid state, Vicat softening point (Vicat hardness), density and porosity. BET surface area measurements indicate that these materials possess small specific surface areas of 0.36–2.3 m^2/g with external surface area of ~0.02 m^2/g. The phenyl-containing hybrids exhibit pronounced hydrolytic stability compared to the methyl- and silica-based analogs. The DMSO and sulfolane solutions of the prepared hybrids are transparent to visible light whereas their cold-compressed discs are optically opaque.

1. Introduction

Transparent, translucent and opaque thin films play a crucial role in the development of new materials for wide range of advanced opto-electronic electro-optics and other optical applications [1–11]. Recent developments in flexible and hard glassy thin films have shown increasing academic and technical interest in chalcogen-derived [12–14], fluorine-containing [15], doped-inorganic conducting oxides [7,16] and organic–inorganic hybrid glassy materials [6,8–10,17–22]. Interestingly, different materials with various bonding characteristics are reported to form glassy thin films via chemical/physical vapor deposition, lattice hardening, spray pyrolysis, solvo-thermal casting and other techniques [1,4–7,23,24]. Unlike inorganic glasses (silicate, borate, phosphate, etc.), which are considered as frozen liquids, organic glasses (polycarbonates (PCs), polymethylmethacrylates (PMMA), cycloolefins, episulfides, polythiols, polyisocyanates, etc.) are essentially versatile polymers that soften at relatively moderate temperatures [1–5,12–14,23,24].

Compared to inorganic glasses, organic/polymer glasses possess numerous advantages such as processability, impact resistance, low cost, dying ability and others. On the other hand, they exhibit serious inherent drawbacks which include poor scratch resistance, color centers, thermal deformation and low refractive indices [1–4]. Moreover, aging processes of organic/polymer glasses result in increasing their density and therefore modifying their stiffness which eventually alter their opto-mechanical properties [1,4,13]. Despite these limitations, organic glasses find wide range of applications extending from commodity-engineering materials (plastic lenses, mirrors, aircraft windows, etc.) to fine opto-electronic and electro-optic devices. In fact, numerous polymers can be made to form vitrified organic glasses but few exhibit long term stability to permit their exploitation in practical applications. In this context, theoretical treatments of such materials are complicated with two important puzzling questions. First, why certain materials tend to form glasses irrespective of their bonding characteristics (H-bonding, π-stacking, covalent bonding, ionic and combined)? Second, what structural/physical factors may influence the morphology of materials that lead to the formation of tough/flexible glassy materials rather than crystalline? [1–7,23,24]

The inherent limitations of both organic and inorganic glasses have accelerated the quest for novel organic–inorganic hybrid materials that exhibit glass properties. The great advantage of such hybrid glasses is that their composition, structure and morphology can be modulated to achieve the desired properties [9,24–27]. Furthermore, the high sol–gel synthetic versatility of these materials permits the formation of a wide variety of functional and bifunctional materials at moderate temperatures for exploitation in electroluminescent, photochromic, nonlinear

* Corresponding author. Fax: +962 2 7201071.
E-mail address: isamaraf@just.edu.jo (I. Arafa).

0022-4596/$ - see front matter © 2009 Elsevier Inc. All rights reserved.
doi:10.1016/j.jssc.2009.05.037

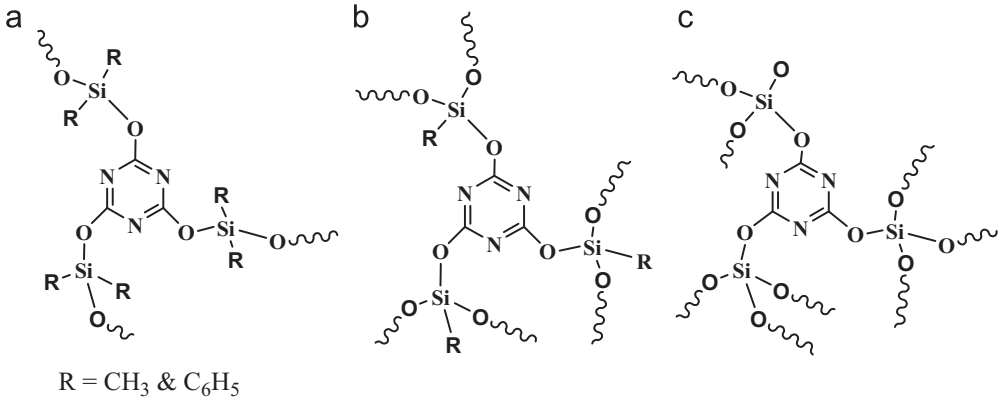

Fig 1. Schematic structures of the prepared (a) bi-, (b) tri- and (c) tetra-functional s-triazine-organosilane hybrid materials.

optics, sensor and other Hi-Tech devices. Literature review on organic–inorganic hybrid glassy materials reveals that research efforts in this area have mainly focused on silica-/functionalized-silica-acrylate, polyimide and other organic-polymer derived hybrid materials [9–11,17–22,28,29]. Even though s-triazine-based resins are extensively used in materials science and technology such as melamine and *p*-phenylene-diisocyanate-cyanuric acid [30–33], few studies and patents have been concerned with s-triazine-silica and s-triazine-organosilane-derived hybrid materials [34,35]. In this paper, we describe our efforts towards the synthesis of a family of hybrid materials composed of s-triazine and different organosilane building blocks as shown in Fig. 1. It is obvious that these hybrid materials rely on using s-triazine as a cross-linking moiety. These new hybrid materials were prepared by one-pot reaction of cyanuric chloride, $(C_3N_3)Cl_3$ with bi-functional R_2SiCl_2, tri-functional $RSiCl_3$ and tetra-functional $Si(OC_2H_5)_4$ organosilanes ($R = CH_3$, C_6H_5) in ethanol. The obtained hybrid materials were characterized using a variety of thermal (TGA), spectroscopic (UV–vis, FT-IR), powder X-ray diffraction (P-XRD) and microscopic (SEM) techniques. Their hydrolytic stability, optical properties, surface porosity and other physical characteristics were also investigated.

2. Experimental

2.1. Materials and methods

All chemicals and solvents were of reagent grade and used as received without further purification unless otherwise stated. Reagent grade trichlorocyanuric acid ($C_3N_3Cl_3$, Aldrich), organosilanes ($(CH_3)_2SiCl_2$, CH_3SiCl_3, $(C_6H_5)_2SiCl_2$, $C_6H_5SiCl_3$), $Si(OC_2H_5)_4$ (Acros Organics) and triethylamine (Aldrich) were used in all preparations.

UV–visible spectra were obtained in DMSO using a Shimadzu double beam UV–vis spectrophotometer UV-2401 (PC). FT-IR spectra were recorded on a Nicolet Impact 410 FT-IR spectrophotometer as KBr pellets. Thermogravimetric analysis (TGA) was carried out under nitrogen atmosphere (temperature range = 25–500 °C, heating rate = 10 °C/min) on a Shimadzu TGA-50 system equipped with a computerized data station TA-5 WS/PC, respectively. Powder X-ray diffraction was obtained on a Philips, PW 1729 X-ray diffractometer interfaced with a computer control unit model PW 1710 using Co$K\alpha$1 ($\lambda = 1.789$ Å) generated at 35 kV (40 mA) and the angular range of $2\theta = 5$–100° with 0.02° increments. The positions of the peaks were determined by curve-fitting procedure of the experimental XRD data using Table Curve-2D software (Lowess Algorithm). The textural morphology of the obtained hybrid materials were investigated on SEM-FEI Philips microscope. The samples were sputter-coated with gold (1200, 20 kV, Polaron E6100). Vicat softening points (Vicat hardness) were determined by monitoring the mechanical compressibility of the obtained hybrid materials as a function temperature. The porosity of these materials was obtained using Nova 2200 high speed gas sorption analyzer at liquid nitrogen temperature (77 K).

2.2. Sol–gel synthesis of s-triazine-organosilane hybrid materials

All these macromolecules were prepared by mixing ($C_3N_3Cl_3$) with the desired molar ratio of R_xSiCl_{4-x} ($R = CH_3$, C_6H_5, $x = 2$, 3) or $Si(OC_2H_5)_4$ reagents in absolute ethanol enriched with water at a later stage of the sol–gel reaction process. Thermal treatment of the resulting materials eventually leads to the formation of the desired s-triazine-organosilane networks.

s-Triazine-OSiMe: $C_3N_3Cl_3$ (18.41 g, 100 mmol) is mixed with CH_3SiCl_3 (14.96 g, 100 mmol) in ~250 mL of absolute ethanol at room temperature. A vigorous reaction accompanied by evolution of HCl is observed. After the reaction mixture was left to equilibrate at room temperature, 3–5 mL of water was added followed by rapid mixing. Immediately a white product starts to form. After ~60 min, triethylamine is added to the reaction mixture to neutralize the remaining HCl. The mixture is left overnight to mature. The resulting white solid was filtered off, washed with ethanol and finally dried in a drying oven at ~100 °C for 3–7 days. Yield: 13.5 g. Color/state: white fine powder. FT-IR (KBr disc, cm^{-1}): 3211–3027 (ν_{O-H}), 2880–2774 (ν_{C-H}), 1462, 1401($\nu_{triazine}$), 1270 (δ_{Si-CH_3}), 1123, 1049 ($\nu_{Si-O-Si}$), 1021 (ν_{Si-OH}) and 841 (ν_{Si-CH_3}). UV–visible (DMSO, nm): 286, 283, 277 and 272 nm.

s-Triazine-OSiMe$_2$: This network is prepared as described above using $C_3N_3Cl_3$ (18.41 g, 100 mmol) and $(CH_3)_2SiCl_2$ (19.36 g, 150 mmol). Yield: 16.6 g. Color/state: white soft rubbery solid. FT-IR (KBr disc, cm^{-1}): 3190–3019 (ν_{O-H}), 2962–2774 (ν_{C-H}), 1466, 1397 ($\nu_{triazine}$), 1266 (δ_{Si-H_3}), 1090, 1053 ($\nu_{Si-O-Si}$), 1021(ν_{Si-OH}) and 866 (ν_{Si-CH_3}). UV–visible (DMSO, nm): 286 and 277 nm.

s-Triazine-OSiPh: This product is prepared as shown previously using $C_3N_3Cl_3$ (18.41 g, 100 mmol) and $C_6H_5SiCl_3$ (21.16 g, 100 mmol). Yield: 22.1 g. Color/state: off-white coarse powder. FT-IR (KBr disc, cm^{-1}): 3211–3019 (ν_{O-H}), 2888–2774 (ν_{C-H}), 1466, 1393 ($\nu_{triazine}$), 1432, 1139 ($\delta_{Si-C_6H_5}$), 1053 ($\nu_{Si-O-Si}$) and 996 ($\nu_{Si-OH)}$. UV–visible (DMSO, nm): 285, 278, 271 and 264 nm.

s-Triazine-OSiPh$_2$: This hybrid network was prepared using $C_3N_3Cl_3$ (18.41 g, 100 mmol) and $(C_6H_5)_2SiCl_2$ (38.0 g, 150 mmol).

Yield: 20.8 g. Color/state: creamy-white sticky hard rubber. FT-IR (KBr disc, cm^{-1}): 3411–3052 (ν_{O-H}), 2870–2778 (ν_{C-H}), 1475, 1397 ($\nu_{triazine}$), 1430, 1123 ($\delta_{Si-C_6H_5}$), 1033, 1020 ($\nu_{Si-O-Si}$) and 997 (ν_{Si-OH}). UV–visible (DMSO, nm): 284, 278, 272 and 266 nm.

s-Triazine-SiO_2: This network was prepared following similar procedure as shown above using $C_3N_3Cl_3$ (18.41 g, 100 mmol) and $Si(OC_2H_5)_4$ (15.60 g, 75 mmol). Yield: 15.2 g. Color/state: white coarse powder. FT-IR (KBr disc, cm^{-1}): 3211–3027 (ν_{O-H}), 1458, 1393 ($\nu_{triazine}$), 1188, 1053 ($\nu_{Si-O-Si}$) and 948 (ν_{Si-OH}). UV–visible (DMSO, nm): 286, 283, 278 and 272 nm.

3. Results and discussion

3.1. Synthesis and characterization

Sol–gel method is a widely employed synthetic technique for the preparation of Si-based hybrid materials [24–27]. The adopted synthetic procedure in the preparation of these hybrid materials is summarized in Scheme 1. This process is known to occur through several intermediate steps involving the formation of ethoxy/hydroxy derivatives of the organosilane and cyanuric acid, Eqs. (1) and (2). These derivatives are expected to self-organize into non-covalent complex networks:

$$R_2SiCl_2 + 2C_2H_5OH \xrightarrow{-2HCl} R_2Si(OC_2H_5)_2 \xrightarrow{H_2O} R_2Si(OH)_2 + R_2Si(OC_2H_5)(OH) \quad (1)$$

$$C_3N_3Cl_3 + 3C_2H_5OH \xrightarrow{-3HCl} C_3N_3(OC_2H_5)_3 \xrightarrow{H_2O} C_3N_3(OH)_3 + C_3N_3(OC_2H_5)_2(OH) + C_3N_3(OC_2H_5)(OH)_2 \quad (2)$$

exploiting the available non-covalent H-bonding, π-stacking and other hydrophobic interactions as depicted in Scheme 2. Equilibration of the resulting self-assembly leads eventually to the formation of thermodynamically stable associated hybrid materials [36–39]. At this stage, the bonding within s-triazine-organosilane networks is mostly physical in nature but further heat treatment eventually leads to condensation, gelation and ultimately the conversion of non-covalent physical architectures into covalently bonded chemical continuous networks. In fact, thermal treatment at 100–150 °C under vacuum to a constant weight was employed to ensure that thermodynamically stable architectures are formed with maximum cross-linking. These hybrid materials are soluble in hot DMF and DMSO but insoluble in most of organic solvents.

A summary of some important physical characteristic data for the prepared s-triazine-organosilane hybrid materials including their state, bulk density and BET porosity measurements are listed in Table 1. The tri- and tetra-functionalized silica (s-triazine-OSi*R*, s-triazine-SiO_2) hybrids exhibit similar bulk density values of 1.67 g/cm^3, whereas that of the bi-functional s-triazine-OSiR_2 analogs was found to range from 1.26 g/cm^3 for the methyl-derived network to 2.47 g/cm^3 for the phenyl-based analog. This observation implies that the tri- and tetra-functional derivatives present similar packing properties. On the contrary s-triazine-$OSiMe_2$ which exhibits a loose packing structure with significant void volume, the s-triazine-$OSiPh_2$ networks display a densely packed structure. In fact, density measurements are in accordance with SEM micrograph images, see SEM section. It should be pointed out that BET measurements on these materials indicate that they posses small specific surface areas of 0.36–2.3 m^2/g with external surface area of ~0.02 m^2/g. However, their porosity values, as indicated by the average pore diameter, show that these hybrids are mesoporous in nature (2 nm, microporous $< d <$ 50 nm, macroporous).

3.2. FT-IR spectroscopy

FT-IR is a very useful technique to examine organic–inorganic interfacial interactions and to determine the extent of condensation reactions. The spectra for the obtained s-triazine-organosilane hybrids were recorded in the region of 4000–400 cm^{-1} as KBr pellets. The observed FT-IR bands and their assignments are reported in the experimental section [40,41].

It is obvious from the spectra in Fig. 2 that these hybrid materials exhibit 2–3 overlapping broad bands in the range 3000–3200 cm^{-1}. These bands are characteristic of the ν_{O-H} which can be due to unreacted silanol (≡Si–OH), hydroxyl (s-triazine-OH) groups and structural water adsorbed and/or occluded in the formed networks. The relatively high intensities of these bands suggest incomplete formation of the network structures. The presence of trace amounts of ethanol/water embedded in network structures is supported by TGA observations where the mass loss due to adsorbed volatile ethanol/moisture (below 100 °C) is negligible, whereas those entrapped in the structure are lost at about 150 °C, see data on TGA.

As seen in Fig. 2, methylsilane-containing hybrid materials exhibit typical infrared absorption bands in 1266–1270 and 841–866 cm^{-1} regions ascribed to (δ_{Si-CH_3}) and (ν_{Si-CH_3}), respectively [40]. However, the phenylsilane-derived analogs display their corresponding infrared absorption bands at 1429–1432 and 1123–1140 cm^{-1}. Furthermore, the diagnostic infrared bands due to s-triazine rings are clearly observed in 1600–1400 cm^{-1} range in all FT-IR spectra of the obtained networks [41]. It is noteworthy to say that the structural information deduced from infrared

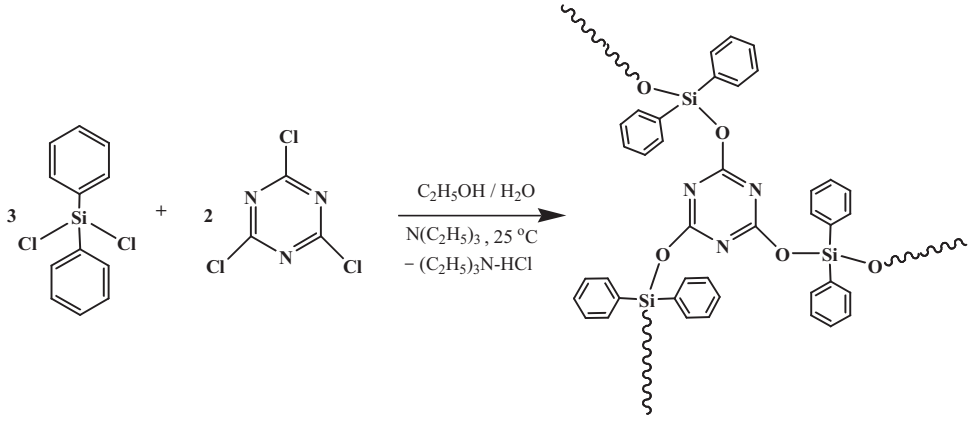

Scheme 1. Sol–gel scheme for the formation of s-triazine-organosilane hybrid materials.

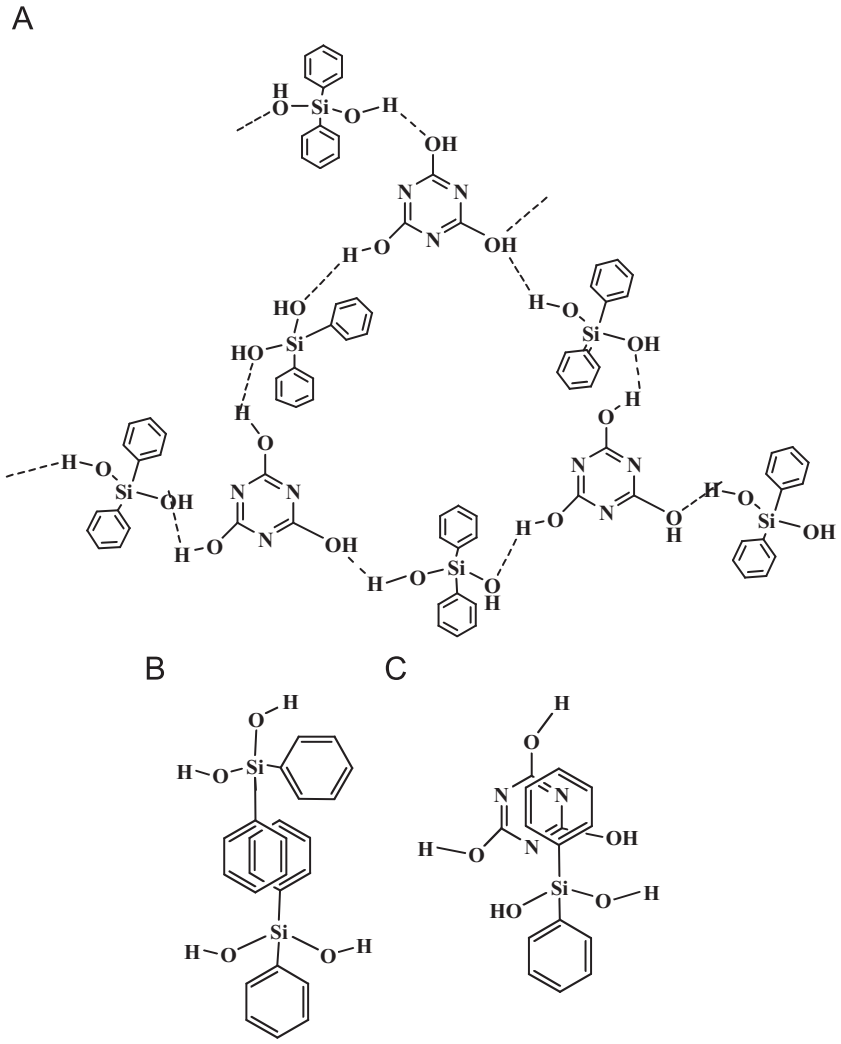

Scheme 2. H-bonding (A), phenyl–phenyl (B) and phenyl-s-triazine (C) π-stackings involved in s-triazine-organosilane supramolecular self-assembly.

Table 1
A summary of the physical characteristics data for the prepared s-triazine-organosilane hybrid materials.

s-Triazine-organosilane	**State**	**Density**[a] (g/cm^3)	**BET**[b] **surface area** (m^2/g) specific (external)	**Porosity**[c]	
				Pore vol. (ml/g)	Diameter (nm)
s-Triazine-OSiMe	Powder	1.67	2.3 (0.02)	3.8×10^{-3}	6.8
s-Triazine-$OSiMe_2$	Rubbery	1.26	N[d]	N[d]	N[d]
s-Triazine-SiO_2	Powder	1.67	0.36(0.02)	0.6×10^{-3}	6.2
s-Triazine-OSiPh	Powder	1.66	0.75(0.02)	1.4×10^{-3}	7.4
s-Triazine-$OSiPh_2$	Rubbery	2.47	N[d]	N[d]	N[d]

State, density, BET surface area, porosity and Vicat softening point.

[a] Bulk density for settled particles in ethanol.
[b] Specific (external, ASTM D5816) surface area are obtained from BET measurements.
[c] Total pore volume and average pore radius are obtained from BET measurements.
[d] The rubbery structures showed negligible BET and porosity values.

spectroscopic data is complemented with the information gathered from thermal and X-ray diffraction measurements.

3.3. Electronic spectroscopy

The UV–visible spectra for the obtained s-triazine-organosilane hybrid materials were recorded in DMSO. All these hybrid materials do not show any absorption in the 800–300 nm range which implies that these networks are transparent in the UV–A–visible region, Fig. 3. However, the methylsilane- and silica-based hybrid materials exhibit two main electronic absorption bands (286–271 nm) assigned to n–π^* and π–π^* s-triazine localized transitions. Each of these transitions is split into two clearly resolved maxima suggesting the presence of s-triazine ring in two different spatial configurations. However,

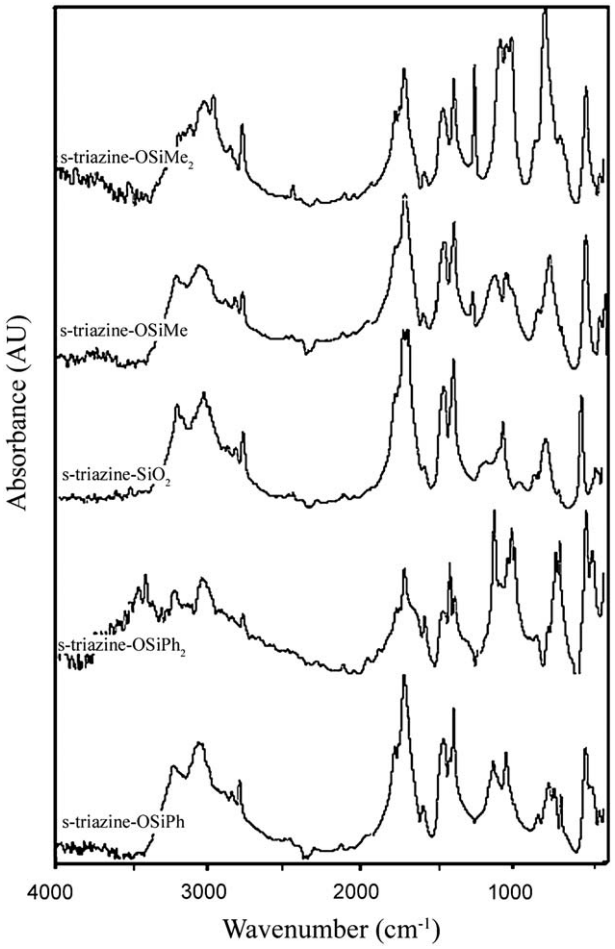

Fig. 2. FT-IR spectra for the synthesized s-triazine-organosilane network structures.

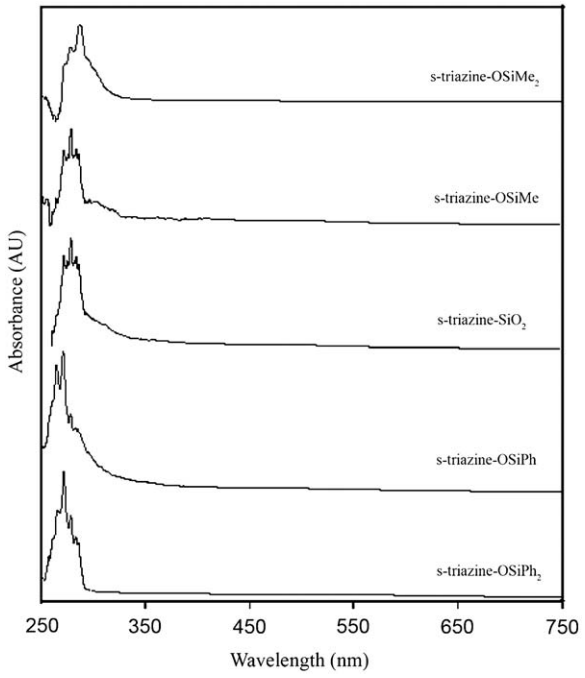

Fig. 3. UV–visible spectra of the prepared s-triazine-organosilanes in DMSO.

the phenylsilane-based hybrid materials display an additional single sharp peak at ~265 nm due to the localized π–π^* transition on the pendent phenyl group.

3.4. Thermal analysis

The thermal behavior of the prepared s-triazine-organosilane hybrid materials was examined using thermogravimetric analysis under N_2 atmosphere in the temperature range of 25–500 °C and heating rate of 10 °C/min. The thermal stability of these materials as evaluated from TGA data is summarized in Table 2. It is clear from the corresponding thermogram curves depicted in Fig. 4a that negligible mass loss (<0.5%) occurred below 150 °C which indicates that negligible adsorbed/occluded moisture and ethanol are entrapped in their network structures. The small degradation step (3–7%) observed in the 180–220 °C range suggest elimination of structural water from vicinal/neighbouring OH groups of uncondensed silanol and cyanuric acid functionalities leading to further structural curing of the hybrid network.

In general, the TGA thermal data shows that the network structures of these materials degrade in the temperature range of 348–370 °C leaving behind silica, organosilane and carbonaceous residues. Close inspection of the observed major degradation step and its first derivative shows that this major step is composed of three poorly resolved steps which are ascribed to the loss of s-triazine building blocks, Fig. 4b. In this context, it is well documented that s-triazine derivatives such as cyanuric acid, $C_3N_3(OH)_3$, exhibit a single decomposition step at ~370 °C to a volatile isocyanic acid, HN = C = O, with 0% char formation [41]. Interestingly, the tri-functional s-triazine-OSiMe and s-triazine-OSiPh hybrids gave the higher residue yield compared to the bi- and tetra-functional analogous hybrids. Furthermore, the average thermal degradation rate in μg mass loss per second was estimated from the slope of the curve. It is obvious that the s-triazine-SiO_2 hybrid decomposed at a rate of 9.7 μg/s whereas others degrade at slower rates (4.8–6.7 μg/s).

Typically, a material softness/hardness can be inferred from its glass transition (T_g) values and/or Vicat softening temperatures (VST) [42]. Since the VST is generally employed for thermal processing of thin films we report the softening temperatures of these hybrid materials as measured by the Vicat method (ASTM D1525). It is obvious from the data in Table 2 that these hybrid materials exhibit a wide range of VSTs. Close examination of these values shows that s-triazine-OSiMe hybrid soften over a broad range of 73–146 °C which implies that this hybrid contains soft-hard domains within its network structures. Meanwhile the other hybrids cover a relatively smaller range of 10–30 °C. These VSTs and ranges permit the synthesis of s-triazine-organosilane hybrid materials with modulated hardness using the proper choice of organosilane mixtures and their molar ratios. In this context, it is essential to point out that hard glassy polymers such as polycarbonate, polymethylmethacrylates and poly(ethyleneterephthalate (PET) exhibit VSTs of ~164, ~103 and ~261 °C, respectively [42].

Interestingly, these hybrid materials exhibit different thermo-oxidative behaviors when subjected to flame pyrolysis tests in air, while the silica-based hybrid decomposes to give a white silica residue with no observable smoke, the methylsilane derivatives give flameless white fumes with white-grey residues and the phenylsilane derivatives give white smoke with black carbonaceous residues. In all cases these hybrid materials exhibit self-extinguishing properties. This test demonstrates that these networks can be exploited as self-extinguishing fillers.

Table 2
Thermogravimetric data for the prepared s-triazine-organosilane hybrid materials.

s-Triazine-organosilane	Degradation temperature[a] °C (% mass loss)[b]			Residue (%)	Degradation rate[c] μg/s[d]	Softening[e] point °C
	Step 1	Step 2	Step 3			
s-Triazine-OSiMe	190 (7)	350 (58)	–	35	6.7	73–146
s-Triazine-OSiMe$_2$	205 (3)	370 (60)	460 (20)	17	5.5	<25
s-Triazine-SiO2	180 (3)	360 (80)	–	17	9.7	170–180
s-Triazine-OSiPh	–	348 (52)	–	48	4.8	119–140
s-Triazine-OSiPh$_2$	220 (3)	362 (70)	–	27	5.7	56–86

[a] TGA was recorded in the temperature range of 30–500 °C (heating rate = 10 °C/min, N_2 atm., degradation temperature is recorded as mid point).
[b] % mass of adsorbed volatile and moisture lost below 150 °C are <0.5%.
[c] The average thermal degradation rate (μg/s) was calculated from the slope of the curve.
[d] % mass of the residues is reported at 500 °C.
[e] Vicat softening point (Vicat hardness, ASTM D1525) refers to the temperature at which the material is penetrated by a flat ended needle (1 mm^2).

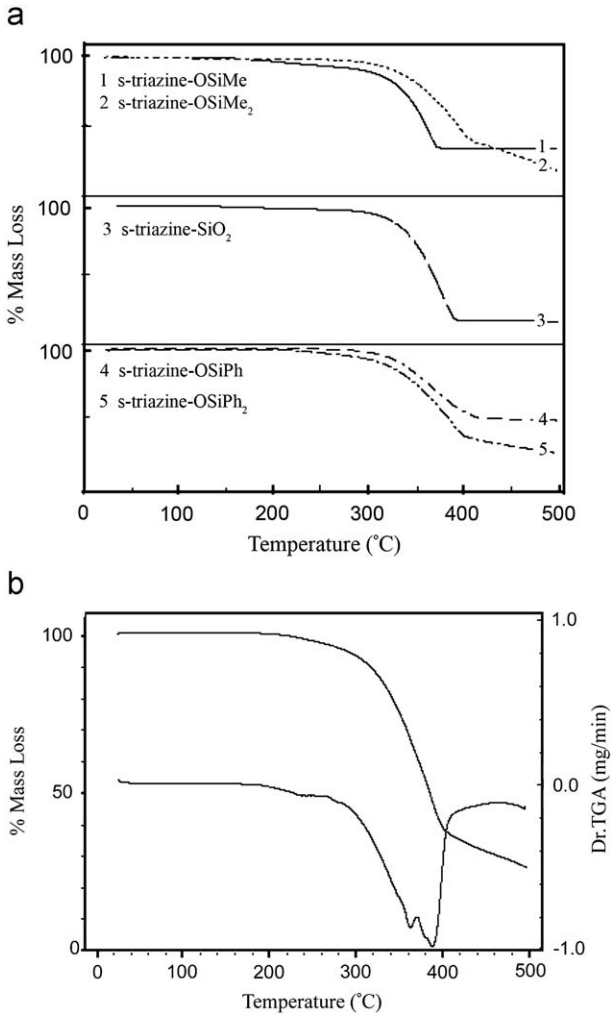

Fig 4. (a) TGA thermograms for the obtained s-triazine-organosilane networks and (b) TGA thermograms of s-triazine-OSiPh$_2$ network and its first derivative.

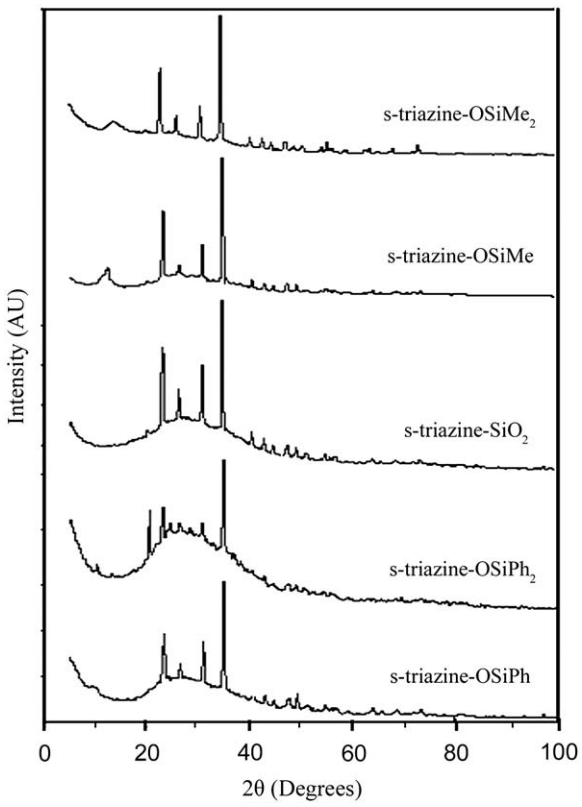

Fig. 5. XRD profiles obtained for the synthesized s-triazine-organosilane hybrid materials.

3.5. Powder X-ray diffraction

Fig. 5 displays the P-XRD profiles obtained for the synthesized s-triazine-organosilane hybrid materials. These profiles show that they are composed of two broad features superimposed with four characteristic sharp diffraction peaks, Table 3. In principle, the P-XRD of methylsilane-based hybrids are mainly composed of sharp diffraction patterns which indicate that they are mostly crystalline in nature, whereas the phenylsilane- and silica-based analogs exhibit broad diffraction features due to their amorphous microstructures. The percentage crystallinity in their structures were evaluated from relative peak areas of P-XRD profiles and found to vary from 15% to 45%, Table 3. Careful analysis of these diffraction profiles shows that they belong to one intact phase which rules out the presence of biphasic organosiloxane-cyanuric acid composite structures [41,43,44]. However, these intact phases may involve both covalent framework and non-covalent adduct structures [16,18,25,30,34–39]. This conclusion is strongly supported by TGA where one major degradation event is observed at 348–370 °C range, and the SEM images which display uniform textural features at 5000× magnification. The corresponding interspatial distances (d-spacing) calculated from Bragg's Equation ($n\lambda = 2d\sin\theta$) for the most intense sharp peak are

Table 3
P-XRD data for the prepared s-triazine-organosilane hybrid materials.

s-Triazine-organosilane[a]	2θ (deg)		d-Spacing (Å)	Particle size[b] (Å)	% Crystallinity
	Broad	Sharp			
s-Triazine-OSiMe	12.2, 27.3[b]	23.1, 26.1, 30.6, 34.9	3.8	8.1	45
s-Triazine-$OSiMe_2$	13.8, 22.4[b]	22.9, 26.1, 30.1, 34.6	5.1	6.7	41
s-Triazine-OSiPh	9.6, 27.4[b]	23.3, 26.3, 31.0, 35.0	3.8	6.1	30
s-Triazine-$OSiPh_2$	10.3, 28.3[b]	20.5, 23.1, 24.4, 26.5, 30.8, 34.8	3.8	6.0	15
s-Triazine-SiO_2	28.3[b]	22.9, 25.9, 30.6, 34.6	3.7	5.4	21

[a] Cyanuric acid phase gives five characteristic peaks at 2θ of 21.5°, 29.3°, 31.7° and 42.7° [41]. The first three diffraction peaks are of almost equal intensity. However, silica phase exhibits a broad diffraction peak at 2θ of ~23.6° [44].
[b] Refers to the broad diffraction peak for which particle size is calculated.

summarized in Table 3. Interestingly, these hybrid materials exhibit similar interplanar spacing of ~3.8 Å except that of the s-triazine-OSiMe[2] which shows a *d*-spacing of 5.1 Å. The relatively small interplanar packing distances of 3.8 Å is indicative of strong π–π interactions between the adjacent aromatic triazine/phenyl rings [41,43,44]. In fact the relatively large *d*-spacing in s-triazine-$OSiMe_2$ hybrid is in accordance with its low density values of 1.26 g/cm^3 and soft rubbery state. This observation implies that the two methyl groups in s-triazine-$OSiMe_2$ adopt a spatial configuration that requires larger free volume than that in s-triazine-OSiMe hybrid. However, the relatively small interspatial spacing in the phenyl-containing hybrids suggests appreciable π–π stacking as depicted in Schemes 2B and C. This conclusion is strongly supported by the SEM images of these materials.

Furthermore, using Scherrer's Equation (shown below) and from the P-XRD data one can calculate the particle size dimension (*L*) of these materials:

$$L = \kappa\lambda/\beta\cos\theta$$

where λ (Å) is wavelength of the X-ray beam, β in radian is the width of the main broad peak at half-height, θ is the diffraction angle and κ = 0.9 is Scherrer's constant. In this group of materials the estimated particle diameters are in the range of 5.4–8.1 Å which suggest the formation of small sized particles. SEM images, however, reveal the formation of microscopic globular or two extended particle aggregates with varying dimensions (5–100 μm). These values imply that such aggregation appears to be strongly influenced by non-covalent intra-particle physical interactions (H-bonding, π-stacking and other hydrophobic bonding types) [45,46].

3.6. Textural morphology

The textural morphology of the obtained s-triazine-organosilane hybrid materials was examined by scanning electron microscopy (SEM), Fig. 6. Their SEM images at low magnifications (1000×) show that they exhibit two different textural features; namely, globular (s-triazine-OSiMe, s-triazine-$OSiPh_2$ and s-triazine-SiO_2) or extended two-dimensional (2-D) network structures (s-triazine-$OSiMe_2$ and s-triazine-OSiPh). However, it is obvious that at large magnifications (5000×) the SEM micrographs indicate that these materials posses different degrees of crystalline characteristics with varying macro-void volumes. Interestingly, their SEM micrographs point out to the presence of one-phase materials in accordance with our P-XRD observations. In this group of materials, significant packing differences are obvious from their SEM micrographs.

The s-triazine-OSiMe SEM image indicates that this hybrid is composed of one-phase of loosely connected globular particles with 5–10 μm in dimension. Close examination of these particles show that they posses internal micropores (2–5 μm) with relatively large inter-particle macrovoids (10–25 μm). However, the SEM micrograph of s-triazine-$OSiMe_2$ indicates that its morphology is made of 2-D fused crystalline particles that are irregular in shape and size (10–100 μm). Surprisingly, the phenyl-based materials exhibit dramatic different textural morphologies where s-triazine-OSiPh is made up of irregular compact-fused 2-D particles while the s-triazine-$OSiPh_2$ is composed of practically regular particles (~5 μm) with inter-particle void volume of ~1 μm. However, s-triazine-SiO_2 particles show globular textural features composed of inter-connected small particulates (~1 μm) encompassing inner pores of ~1–5 μm.

3.7. Properties

The hydrolytic stability of the obtained s-triazine-organosilane networks was examined by monitoring the pH of their suspensions in water under neutral conditions. Indeed, partial hydrolysis of the ≡Si–O–C≡ structural units in the backbone resulted in the formation of silanol (≡Si–OH) and cyanuric acid (≡C–OH) groups with no apparent breakdown of the network structures when left in contact with water for a period of 24 hours, Eq. (3) [34,47]. The phenyl-containing hybrids show exceptional stability compared with the methyl-derived and silica-based hybrids in neutral and acidic media but not in basic medium. This observation can

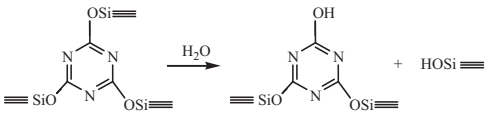

(3)

be explained by considering the hydrophobic nature of the phenyl group which does not allow water to penetrate deep in the network structure [48]. It is essential to point out that the hydrolyzed moiety can be regenerated thermally with the elimination of water between adjacent groups [18,34,49]. This attractive self-healing feature is under further investigation.

The partial amorphous/crystalline nature of these materials combined with their small surface areas (specific surface area = 1–2 m^2/g, external surface area ~0.02 m^2/g) motivated us to examine their tendency to form glassy thin films by solvothermal methods (<250 °C) and study their optical properties. Thus we were unable to form sufficiently uniform thin films of these materials to study their optical characteristics. The poor thin films forming ability of these hybrids may be attributed to the relatively high surface energies of the obtained particles due to the presence of uncondensed OH groups, see FT-IR section. This has hindered our current efforts to examine their solid state optical properties. It is often noted that in thin film formations the

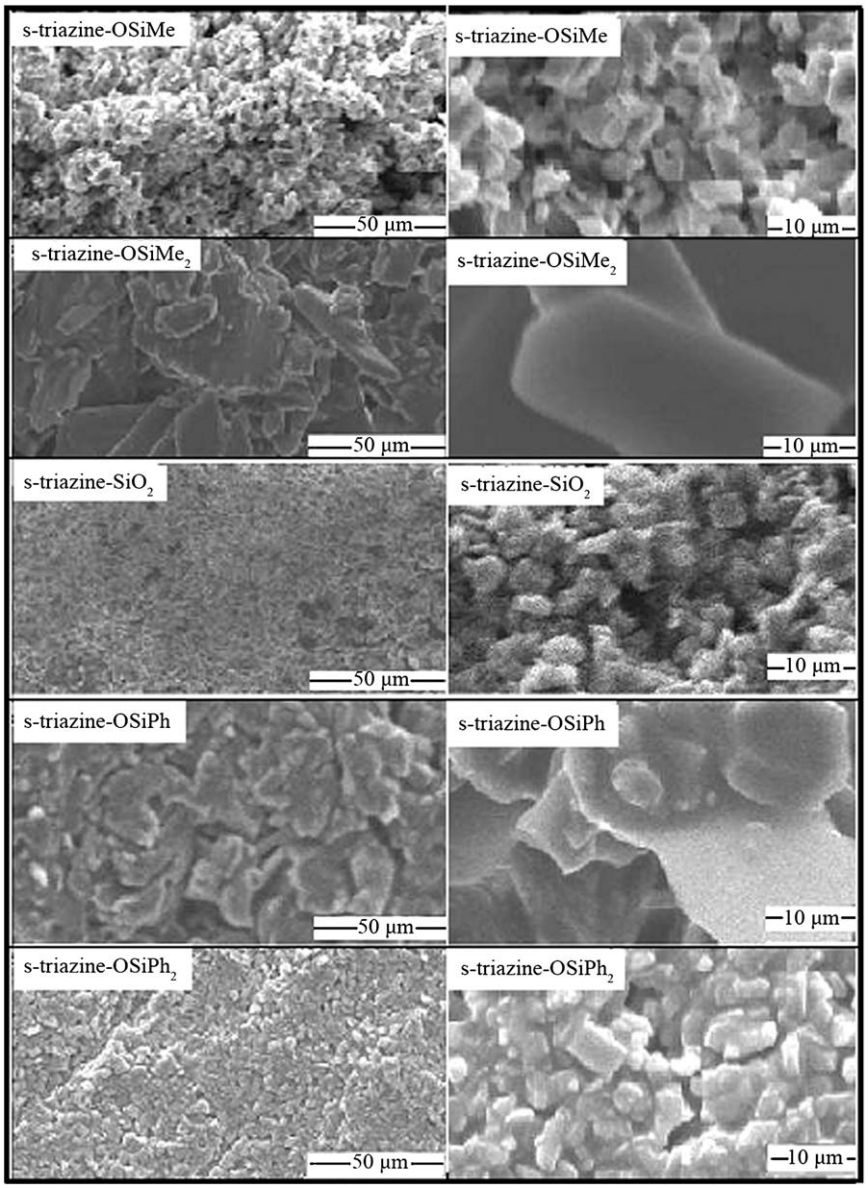

Fig. 6. SEM images ($x = 1000$ and 5000) of the synthesized s-triazine-organosilane hybrid materials.

moisture in the lattice domain, lattice perturbation due to random cross-linking and the presence of OH groups can lead to high scattering of light [4,24,50]. These structural factors are crucial to the overall thin film quality, such as transparency, consistency and other optical properties. To overcome solvent pitting and to enhance particle–particle interfacial interactions by lowering their surface energies two approaches were attempted. First, by minimizing the number of unreacted OH groups via partial fluorination and the second involves using non-ionic surfactant–solvent system. In both approaches, improvement of the thin film quality is observed but not to a satisfactory level.

4. Conclusions

This work is part of our continuing efforts to generate triazine-organosilane hybrid materials that will pave the road for developing novel hybrid materials for wide range of applications [51]. Based on the structural information gathered from FT-IR, TGA, P-XRD and SEM the obtained s-triazine-organosilane hybrid networks can be described as lamellar-globular 2–3D networks composed of s-triazine and organosilane building blocks. Furthermore, inter- and intra-particle physical interactions such as H-bonding, π-stacking and other hydrophobic interactions play a crucial role in the overall bonding characteristics in this family of hybrid materials. Attempts to form high quality thin films of these materials have been hindered apparently by the presence of uncondensed OH groups. Overcoming this obstacle is crucial to prevent pitting by the different solvent systems employed in thin films formations. However, the inability of these materials to form homogeneous fully interconnected intact thin films can be treated at different levels of sophistication. Our future work focuses on modulating the structure of these hybrids by selectively introducing allyl functionality on the s-triazine building block, and further allowing it to undergo Diels–Alder cycloaddition reactions with the goal of glass formation through lattice hardening technique.

Acknowledgment

Financial support from the Deanship of Research at the Jordan University of Science and Technology is gratefully acknowledged.

References

[1] M.-C. Choi, Y. Kim, C.-S. Ha, Prog. Polym. Sci. 33 (2008) 581–630.
[2] L. Nicole, C. Boissière, D. Grosso, A. Quach, C. Sanchez, J. Mater. Chem. 15 (2005) 3598–3627.
[3] E. Coronado, E. Palomares, J. Mater. Chem. 15 (2005) 3593–3597.
[4] W.A. MacDonald, J. Mater. Chem. 14 (2004) 4–10.
[5] K.G. Sharp, J. Mater. Chem. 15 (2005) 3812–3820.
[6] N. Umeda, A. Shimojima, K. Kuroda, J. Organomet. Chem. 686 (2003) 223–227.
[7] A.N. Banerjee, K.K. Chattopadhyay, Prog. Cryst. Growth Charact. Mater. 50 (2005) 52–105.
[8] P. Innocenzi, B. Lebeau, J. Mater. Chem. 15 (2005) 3821–3831.
[9] Y. Kamimura, K. Kurumada, J. Non-Cryst. Solids 353 (2007) 2521–2527.
[10] M. Łączka, K. Cholewa-Kowalska, M. Kogut, J. Non-Cryst. Solids 287 (2001) 10–14.
[11] C. Sanchez, B. Lebeau, F. Chaput, J.-P. Boilot, in: P. Gómez-Romero, C. Sanchez (Eds.), Optical Properties of Functional Hybrid Organic–Inorganic Nanocomposites in Functional Hybrid Materials, Wiley VCH, 2004, pp. 122–171.
[12] R. Okutsu, Y. Suzuki, S. Ando, M. Ueda, Macromolecules 41 (2008) 6165–6168.
[13] S.P. Mishra, K. Krishnamoorthy, R. Sahoo, A. Kumar, J. Mater. Chem. 16 (2006) 3297–3304.
[14] R. Fairman, B. Ushkov, Semiconducting Chalcogenide Glass I, Elsevier, Amsterdam, 2004.
[15] B. Ameduri, B. Boutevin, J. Fluorine Chem. 126 (2005) 221–229.
[16] P.C. Angelomé, G.J. de A.A. Soler-Illia, J. Mater. Chem. 15 (2005) 3903–3912.
[17] C. Molina, P.J. Moreira, R.R. Gonçalves, R.A. Sá Ferreira, Y. Messaddeq, S.J.L. Ribeiro, O. Soppera, A.P. Leite, P.V.S. Marques, V. de Zea Bermudez, L.D. Carlos, J. Mater. Chem. 15 (2005) 3937–3945.
[18] C.K. Chan, S.L. Peng, I.M. Chu, S.C. Ni, Polymer 42 (2001) 4189–4196.
[19] B. Menaa, M. Takahashi, Y. Tokuda, T. Yoko, Optic. Mater. 29 (2007) 806–813.
[20] X. Song, X. Wang, H. Wang, W. Zhong, Q. Du, Mater. Chem. Phys. 109 (2008) 143–147.
[21] H. Sugimoto, K. Daimatsu, E. Nakanishi, Y. Ogasawara, T. Yasumura, K. Inomata, Polymer 47 (2006) 3754–3759.
[22] P.S. Chinthamanipeta, S. Kobukata, H. Nakata, D.A. Shipp, Polymer 49 (2008) 5636–5642.
[23] R.C. Ropp, Studies in Inorganic Chemistry: Inorganic Polymeric Glasses, Elsevier, Amsterdam, 1992.
[24] J. Kron, G. Schottner, K.-J. Deichmann, Thin Solids Films 392 (2001) 236–242.
[25] M.F. Ashby, Y.J.M. Bréchet, Acta Mater. 51 (2003) 5801–5821.
[26] J.D. Mackenzie, J. Sol–Gel Sci. Technol. 26 (2003) 23–27.
[27] W.J. Hunks, G.A. Ozin, J. Mater. Chem. 15 (2005) 3716–3725.
[28] S. Sankaraiah, J.M. Lee, J.H. Kim, S.W. Choic, Macromolecules 41 (2008) 6195–6204.
[29] H. Wang, W. Zhong, G. Du, Y. Yang, H. Okamoto, S. Inoue, Polym. Bull. 51 (2003) 63–68.
[30] T.J. Mooibroek, P. Gamez, Inorg. Chim. Acta 360 (2007) 381–404.
[31] V.R. Pedireeddi, D. Belhekar, Tetrahedron 58 (2002) 2937–2941.
[32] S. Cicchi, G. Ghini, S. Fallani, A. Brandi, D. Berti, F. Betti, P. Baglioni, Tetrahedron Lett. 49 (2008) 1701–1705.
[33] Q. Guo, Q. Yang, L. Zhu, C. Yi, S. Zhang, Y. Xie, Solid State Commun. 132 (2004) 369–374.
[34] N.E.A. El-Gamel, M. Schwarz, E. Brendler, E. Kroke, Chem. Commun. (2006) 4741–4743.
[35] J.-W. Kang, D.-S. Lee, H.-D. Park, Y.-S. Park, J.W. Kim, W.-I. Jeong, K.-M. Yoo, K. Go, S.-H. Kim, J.-J. Kim, J. Mater. Chem. 17 (2007) 3714–3719.
[36] B. Boury, in: F. Ganachaud, S. Boileau, B. Boury, (Eds.), Silicon Based Polymers: Advances in Synthesis and Supramolecular Organization, Springer Science, Berlin, 2008, pp. 233–246.
[37] B. Boury, R.J.P. Corriu, H. Muramatsu, New J. Chem. 26 (2002) 981–988.
[38] D.C. Shrrington, K.A. Taskinen, Chem. Soc. Rev. 30 (2001) 83–93.
[39] D. Brandhuber, H. Peterlik, N. Hüsing, J. Mater. Chem. 15 (2005) 3896–3902.
[40] M.A. Schiavon, G.D. Soraru, I.V. Yoshida, J. Non-Cryst. Solids 348 (2004) 156–161.
[41] Y. Chen, Q. Wang, W. Yan, H. Tang, Polym. Degrad. Stability 91 (2006) 2632–2643.
[42] J.A. Brydson, Plastic Materials, seventh ed., Butterworth-Heinemann, London, 1999.
[43] S.Y. Chong, C. Seaton, B.M. Kariuki, M. Tremayne, Acta Crystallogr. B 62 (2006) 864–874.
[44] I.M. Arafa, M.M. Fares, A.S. Barham, Eur. Polym. J. 40 (2004) 1477–1484.
[45] F.J.M. Hoeben, P. Jonkheijim, E.M. Meijer, A.P.H. Schenning, Chem. Rev. 105 (2005) 1491–1546.
[46] R. Gutzler, S. Lappe, K. Mahata, M. Schmittel, W.M. Heckl, M. Lackinger, Chem. Commun. (2009) 680–682.
[47] D.B. Thompson, F. Gonzaga, A.S. Fawcett, M.A. Brook, Silicon Chem. 3 (2008) 327–334.
[48] A.S. Gordetsov, Yu.I. Dergunov, Russ. Chem. Rev. 54 (1985) 1227–1245.
[49] J. Yang, E.G. Wang, Curr. Opin. Solid State Mater. Sci. 10 (2006) 33–39.
[50] A. Ulman, Chem. Rev. 96 (1996) 1533–1554.
[51] M. Shatnawi, W. Al-Mansi, I. Arafa, J. Solid State Chem. 181 (2008) 150–157.